J. Phys. Chem. A, 2009, 113 (52), pp 15006–15015 DOI: 10.1021/jp905110s

TS-1 from first principles.

Aldo Gamba*, Gloria Tabacchi and Ettore Fois

July 22, 2009

Dipartimento di Scienze Chimiche ed Ambientali, University of Insubria, and INSTM,

Via Lucini 3, I-22100 Como (Italy)

Abstract

First principles studies on periodic TS-1 models at Ti content corresponding to 1.35% and 2.7% in weight of TiO_2 are presented. The problem of Ti preferential siting is addressed by using realistic models corresponding to the TS-1 unit cell [$TiSi_{95}O_{192}$] and adopting for the first time a periodic DFT approach, thus providing an energy scale for Ti in the different crystallographic sites in non defective TS-1. The structure with Ti in site T3 is the most stable, followed by T4 (+0.3 kcal/mol), while the less stable structure, corresponding to Ti in T1, is 5.6 kcal/mol higher in energy. The work has been extended to investigate models with two Ti per unit cell [$Ti_2Si_{94}O_{192}$] (2.7%). The possible existence of Ti-O-Ti bridges, formed by two corner sharing TiO_4 tetrahedra, is discussed. By using cluster models cut from the optimized periodic DFT structures, both vibrational (DFT) and electronic excitation spectra (TDDFT) have been calculated and favourably compared with the experimental data available on TS-1. Interesting features emerged from excitation spectra: i) isolated tetrahedral Ti sites show a Beer-Lambert behavior, with absorption intensity proportional to concentration. Such a behaviour is gradually lost when two Ti occupy sites close to each other; ii) the UV-Vis absorption in the 200-250 nm region can be associated to transitions from occupied states delocalized on the framework oxygens to empty d states localized on Ti. Such extended states-to-local states transitions may help the interpretation of the photovoltaic activity recently detected in Ti zeolites.

Part of the "Vincenzo Aquilanti Festschrift"

1 Introduction

TS-1, titanium silicalite, is a porous crystalline material broadly used in industrial plants as a catalyst for hydrocarbons oxidative processes.[1] Since it allows to operate

at mild conditions using hydrogen peroxide as oxygen source and generating water as a by-product, its discovery[2] is considered a milestone in the development of modern heterogeneous catalysts for sustainable technologies. For this reason, TS-1 has been one of the most extensively studied zeolitic materials and much attention is still focused on its unique physico-chemical and reactivity properties. Besides its relevance in catalysis, TS-1 is currently of interest for advanced applications in other fields, such as solar cell technology. Indeed, titanium zeolites have recently been shown to exhibit photovoltaic activity,[3] thus suggesting their use in dye-sensitized solar cells as porous electron-transport materials as an alternative to dense TiO_2 nanoparticles.

From the structural point of view, TS-1 is a zeolite with MFI framework topology.[4] The all-silica phase of MFI, the catalytically inactive Silicalite-1, has a unit cell content corresponding to $[Si_{96}O_{192}]$. The as-synthesized Silicalite-1, containing tetrapropylammonium cation (TPA^+) as structure directing agent (SDA), has an orthorhombic structure.[5] The calcined form of Silicalite-1 has a monoclinic unit cell with α=90.6° (see e.g. Ref.[6]). The catalytically active phase TS-1, which is characterized by a low Ti content (below 3.0% in weight of TiO_2), is orthorhombic.[6] It can be considered a solid solution of TiO_2 in zeolitic SiO_2, where only a small portion of tetrahedral sites (T sites) are isomorphously occupied by Ti. Thus in TS-1, and in general, in titanium zeolites, Ti is surrounded by 4 oxygen atoms in a tetrahedral environment and is therefore undercoordinated with respect to the stable TiO_2 phases, where Ti occupies octahedral sites (TiO_6). Indeed, it is believed that such a Ti fourfold coordination is the actual responsible of Ti zeolites catalytic activity, because TiO_2 contents higher than 3% lead to phase separation of octahedral TiO_2 phases and deactivation of the catalytic properties of the material.[7]

In view of its role in industrial catalysis, TS-1 has been the subject of many experimental investigations carried out with a variety of spectroscopic techniques. In spite of the broad benchmark of UV-Vis, IR, raman, and X-ray data on Ti sites in TS-1 available in

the literature,[8–11] details of the TS-1 structure at the microscopic level are still unclear. One of such issues is concerned with the Ti location in TS-1. Diffraction studies[12–14] suggested a nonrandom distribution of Ti in the tetrahedral T sites of TS-1. However, there is still no general consensus on the T sites actually occupied by Ti in TS-1, and different siting probabilities were reported (see ref.[15]).

The uncertainty in locating Ti is associated with the low Ti concentration, corresponding to approximately 2-3 Ti atoms in the TS-1 unit cell. Moreover, due to its large unit cell size and low Ti content ($[Ti_xSi_{96-x}O_{192}]$), this crystalline catalyst has escaped a thorough theoretical characterization to date. Studies aimed at establishing the location of Ti in TS-1 have been performed only by adopting force-field based schemes[16,17] or quantum mechanical methods on cluster or embedded cluster models (see e.g.[15,18]). Primary goal of this work is to fill this gap, by performing a series of Density Functional Theory (DFT) calculations by using for the first time a first-principles periodic approach for such a large system.

Although the high calcination temperature needed to obtain the active TS-1 catalyst may suggest a role of thermodynamics in ruling the Ti distribution in the different T sites, the microscopic origin of Ti preferential siting is still a matter of discussion, and a series of hypotheses have been formulated (see e.g. Ref.[12,15,19]). It has been proposed that kinetic factors may be the predominant ones in determining the actual Ti location.[15] Also, it has been suggested that, already during the nucleation and growth process, Ti siting may be influenced by the distribution of the structure directing agent, because of the coulomb interactions between positively charged SDAs and pentavalent anionic (hydroxylated) Ti centers detected in as-synthesized (non calcined) TS-1.[19] Moreover, it has been reported that the disappearance of defect centers (e.g. Si-OH groups) correlates with an increase of Ti concentration, suggesting the idea that Ti replaces defective sites in TS-1 .[12] In this scenario, our work is aimed at establishing an energy scale for Ti occupancy in the different tetrahedral sites of TS-1 by using a

periodic DFT approach.

Since in the orthorhombic MFI framework there are 12 crystallographically different tetrahedral sites, geometry optimizations have been carried out on 12 $[TiSi_{95}O_{192}]$ structures obtained by placing Ti in one of the twelve inequivalent T positions. These structures correspond to a title of 1.35% in weight of TiO_2. Optimizations have been also performed on structures characterized by a $[Ti_2Si_{94}O_{192}]$ stoichiometry, in order to explore the energetics of TS-1 models at a 2.7% Ti content. In this case, a systematic computational investigation is prevented by the number of possible structures: as there are 12 T sites, each with multiplicity 8, there are 96!/(2!(96-2)!)=4608 possible structures characterized by different location of 2 Ti atoms. However, relevant insight has been gathered by focusing the analysis on a restricted subset of models, thus enabling to quantify the energy separation among the different Ti distributions for a TS-1 framework characterized by a Ti content close to that typical of the actual catalytic material.

Besides energetic issues related to Ti siting, electronic and vibrational properties of Ti in the different tetrahedral sites of the TS-1 model systems were studied. A thorough analysis has been performed on electronic excitation spectra in the UV-Vis region, where a signature of zeolitic titanium is detected at around 200-250 nm.[20] Moreover, IR and raman spectra were calculated and compared with the corresponding spectroscopic data,[8,9] which also exhibit fingerprints of framework Ti. From such a theoretical characterization of Ti sites, combined with the analysis of their energy stability, reliable predictions about the Ti distribution in TS-1 could be deduced.

2 Methods of calculations and Models

The orthorhombic framework of TS-1 (space group Pmna, see e.g. Ref.[12]) is characterized by interconnected channels, whose section is formed by 10-membered rings. The secondary building unit is a 5-1 structure characterized by a 5-membered ring (5-ring).[4]

There are 12 non equivalent T sites (each with multiplicity 8) and 26 non equivalent O sites (see Figure 1). The twelve possible structures [$TiSi_{95}O_{192}$], identifiable by the location of Ti in one of the 12 sites (labelled T1, T2, T3, .., T12), were studied by adopting plane waves as basis set and the PBE gradient corrected DFT functional.[21] The geometry of each of the 12 [$TiSi_{95}O_{192}$] systems (T1,T2,..T12 from now on) was optimized by using ultra soft Vanderbilt pseudopotentials[22] with a 30 Ry cutoff for the plane waves expansion of the orbitals, and a 180 Ry cutoff for the electronic density (PBE/VDB/30) at the Γ point. Periodic boundary conditions were applied.

Such a computational scheme, based on ultra-soft pseudopotentials and PBE approximation to DFT, has been successfully adopted in the study of the structure and the energetics of large systems, like e.g. TiO_2 surfaces[23] and aluminosilicate porous materials.[24] Moreover, the PBE approximation has proven reliable for the structure and energetics of other heteroatom substituted zeolite structures, like boron zeolites.[25,26]

Optimizations were carried out, using a quasi-Newton scheme, at fixed cell parameters (fixed volume), while no constraint was imposed on the nuclear positions. Optimizations were considered converged when the maximum force on atoms was less than 10^{-4} a.u.. The CPMD code[27] was used for the plane waves periodic DFT calculations. The cell parameters adopted in the calculations (a=20.049 Å, b=19.926 Å, c=13.401 Å), are extracted from diffraction studies on TS-1 with corresponding Ti content.[12] With the same computational setup, we have optimized the structures of few [$Ti_2Si_{94}O_{192}$] models, obtained by placing Ti in two T sites, and adopting cell parameters (a=20.113 Å, b=19.930 Å, and c=13.410 Å) corresponding to a TS-1 sample of comparable Ti content.[12]

For the electronic excitation spectra calculations, two different approaches were adopted. In one, the cluster approach, time dependent DFT (TD-DFT)[28,29] calculations were carried out on Ti containing clusters cut from the PBE/VDB/30 optimized periodic structures. Three cluster models of different size were adopted, namely C_{tetra}, C_{5-ring}

and C_{2tetra}, represented in Figure 1. In the smallest model C_{tetra}, with stoichiometry Ti-[O-($Si(OH)_3$]$_4$, Ti is surrounded by four tetrahedral building units, i.e., by two oxygen atoms shells. Oxygens in the second shell were saturated with H atoms located at 1.0 Å from O, along the O-Si bond direction in the corresponding optimized crystal structure. Cluster C_{5-ring} contains a 5-ring structure and is characterized by a $Ti_xSi_{9-x}O_9(OH)_{18}$ stoichiometry, while C_{2tetra} is formed by two corner sharing C_{tetra} clusters and has a $Ti_xSi_{8-x}O_7(OH)_{18}$ formula. Systems with x=0,1,2 have been considered. The C_{5-ring} and the C_{2tetra} clusters were used, with x=2, to investigate the properties of Ti-O-Si-O-Ti and Ti-O-Ti bridges respectively. The external oxygen atoms were saturated by the same procedure adopted in the C_{tetra} model. TD-DFT excitations were calculated using the hybrid B3LYP functional[30] and a gaussian basis set (6-311+g**).[31] Convergence was required for at least 50 excited states. We shall refer to these results as TDDFT/Cluster.

In a second approach, the electronic excitation spectrum was calculated by adopting periodic boundary conditions. Specifically, the optical conductivity of the PBE/VDB/30 optimized structures was calculated by using the PBE functional and norm conserving pseudopotentials[32,33] with a cutoff of 110 Ry for the plane wave expansion of the orbitals and 440 Ry for the electronic density. In the case of large periodic systems, the more accurate TD-DFT approach for electronic excitations is not viable, however, gradient corrected DFT gives results quite close to TD-DFT in the case of Ti-zeolite systems.[34–36] We shall refer to these calculations as DFT/pbc.

In the calculated electronic excitation spectra, both DFT/pbc and TDDFT/cluster, a line broadening of 2.0 nm was applied.

Vibrational properties, IR and raman, were calculated on the above described cluster models. To this aim, the clusters geometries have been re-optimized using the B3LYP functional and the 6-311g** basis set. In the minimization process, the "external" O-H atoms were kept fixed in order to mimic the constraint due to the full crystal

and to decouple the calculated vibrational spectra from signals due to modes involving O-H groups. Such modes are known to interfere in the silica window, an otherwise transparent region between 850-1000 cm^{-1} typical of SiO_2 materials, where signals of tetrahedral Ti can be found. All the spectra are calculated within the harmonic approximation and obtained from stationary points, characterized by positive frequencies. A line broadening of 10 cm^{-1} was used for both IR and raman spectra representations. As common practice in comparing with experimental data, a shift factor of 0.98 was applied to the calculated wavenumbers.[37]

3 Results

3.1 Structure and Energetics

The minimum energy structure among the twelve $[TiSi_{95}O_{192}]$ models corresponds to the one where Ti occupies site T3. Such a structure is however only 0.28 kcal/mol below the one with Ti in T4, while the highest energy structure, 5.6 kcal/mol above the T3, corresponds to Ti in T1. Therefore it turns out that energy differences among TS-1 systems characterized by 1.35% Ti are within 5.6 kcal/mol. Remarkably, nine out of twelve structures are in the 4 kcal/mol range from the mimimum.

The calculated Ti-O bond distances and O-Ti-O bond angles are reported in Table 1 and Table 2, respectively. It should be said at the outset that all Ti sites have a slightly distorted tetrahedral structure. In general, the calculated Ti-O bond lenghts are in agreement with the value of 1.793 Å reported from in vacuo X-ray spectroscopies studies on calcinated TS-1 samples.[11] The trends of: i) average Ti-O bond distances, ii) Ti-Si (first-neighbors) distances and iii) Ti-O-Si angles as a function of Ti siting in the twelve $[TiSi_{95}O_{192}]$ optimized structures are reported in Figure 2 along with the energy differences ΔE. Also reported in Figure 2 are the (normalized) probability associated to Ti occupancy of the different T sites. Probabilities were calculated, from

the Boltzmann factor exp(-ΔE/kT), for room temperature and for 500°C, a commonly adopted calcination temperature. It can be deduced, on purely energetics grounds, that the T3 and T4 sites would account for more than 50% of Ti even at high calcination temperatures.

Selected configurations with stoichiometry [$Ti_2Si_{94}O_{192}$], corresponding to two Ti per unit cell, have been optimized as well. They represent only a subset of the many possible configurations with such a Ti content. In all cases one Ti (Ti^1) was placed in one T3 site, corresponding to the minimum energy monosubstituted structure, while the location of second Ti (Ti^2) varied, and a total of twenty different configurations were optimized. The Ti^1-Ti^2 pairs, their Ti-Ti distances and the relative stability are graphically represented in Figure 3. The most stable system corresponds to a configuration with Ti^2 in a T4 site at about 7.3 Å from Ti^1. However most of the optimized structures are within 6 kcal/mol from the minimum energy arrangement. It is to notice that the energy difference depends not only on the pair of sites but also on their actual separation. On the other hand, in the case of Ti in T3-T5 two T5 sites are available at similar distances from T3 (at about 5.2 Å), but the two corresponding arrangements differ by 1.3 kcal/mol. This finding indicates that also the details of the Ti centres local environment may affect the relative stability of systems characterized by different Ti distributions.

Two systems containing adjacent T sites, characterized by a Ti-O-Ti bridge and a Ti-Ti distance of $\sim$ 3.5 Å, were also considered: the first one, and most stable of the two, with the second Ti (Ti^2) in T4 and the second structure with Ti^2 in T6. The two structures differ by 4.3 kcal/mol; therefore, also for systems with corner sharing TO_4, the relative energy depends on the pair of T sites actually occupied by Ti. Remarkably, the T3-T4 Ti-O-Ti bridge structure is only 2.7 kcal/mol higher than the most stable system with the same Ti content. Its Ti-O bond distances and O-Ti-O angles, reported in Tables 3 and 4 respectively, are very close to the ones calculated for the systems containing a

single Ti site. This indicates that the formation of a Ti-O-Ti bridge implies only small distortions in the geometry of the TiO_4 units. Moreover, the Ti-O-Ti bonds forming the bridge are the shortest ones among the systems here considered.

3.2 Vibrational analysis

IR and raman spectra have been of overwhelming relevance in unravelling the structure of the Ti sites in TS-1 and related materials (see e.g. ref.[8,9]). An IR feature at 960 cm^{-1} has been associated with Ti in zeolitic tetrahedral sites. Moreover, the intensity of such a band has been proved to be related to the content of tetrahedral Ti in TS-1.[38] Also, a raman signature at 1125 cm^{-1} has been associated to tetrahedral Ti. In Figure 4a the calculated IR and raman predictions are shown for a Ti containing cluster and for the equivalent all-silica one. The spectrum of the T3 centered C_{tetra} system is reported in Figure 4a, along with that calculated for a C_{5-ring} with one Ti in T3. As clusters centered on different crystallographic T sites have very similar vibrational properties, only the T3 case will be discussed. In the small C_{tetra} cluster, a peak at about 980 cm^{-1} (with a shoulder at 1005 cm^{-1}) is associated with the presence of Ti, both in the IR and in the raman predictions. In the larger C_{5-ring} system, the 980 cm^{-1} feature is red-shifted to 958 cm^{-1}. In the raman activity spectrum, the small C_{tetra} cluster shows an intense peak at 1128 cm^{-1}, which is shifted to 1135 cm^{-1} in C_{5-ring}. In both cases, such a raman active mode is related to an in-phase (symmetric) stretching of the TiO_4 unit. It is to point out that the above discussed features are missing in the spectra of an all silica C_{5-ring} cluster reported in Figure 4a for comparison, and should therefore be attributed to the presence of tetrahedral Ti. Remarkably, both IR and raman results are in line with experimental findings.[8,9]

In Figure 4b and 4c, the vibrational spectra calculated for clusters containing two close Ti atoms are shown, one is relative a Ti-O-Ti bridge, the other to a Ti-O-Si-O-Ti structure respectively. Let us discuss the vibrational properties of a C_{2tetra} system containing a Ti-O-Ti bridge (Figure 4b). In the IR spectrum, such a system is char-

acterized by two Ti-related features, at 853 cm^{-1} and at 1006 cm^{-1}, both located at the edges of the silica window. A very intense raman-active peak is found at 1114 cm^{-1}, two weaker raman signals are found at 978 and 1003 cm^{-1}. Also a very weak raman signal is calculated at 853 cm^{-1}. The above IR and raman signals are due to the Ti-O-Ti bridge, as they are missing in the spectra of the other C_{2tetra} clusters, reported in Figure 4b, which do not contain such a bridge.

In the case of a C_{5-ring} characterized by a Ti-O-Si-O-Ti bridge (Figure 4c), the IR signal at 958 cm^{-1} typical of an isolated tetrahedral Ti is enhanced in intensity, however a new feature appears at 908 cm^{-1}. In the raman spectrum, the 1135 cm^{-1} signal typical of isolated Ti is splitted and red-shifted at 1110 cm^{-1}. The 958 cm^{-1} raman feature is red-shifted to 908 cm^{-1} in passing from a C_{5-ring} with only one Ti to a C_{5-ring} with a Ti-O-Si-O-Ti bridge. The above discussed features are absent (both IR and raman) in the all-silica C_{5-ring} system spectra reported in Figure 4c for comparison.

3.3 Electronic excitation spectra

UV-Vis spectra of dry TS-1 and other Ti-zeolites are characterized by a broad absorption band at 200-250 nm,[9,20,39] which is considered the fingerprint of tetracoordinated Ti in the zeolite framework. Band profiles, as well as maximum position and intensity, slightly vary among the wealth of available experimental data: for instance, a 208-210 nm peak position is reported for dry TS-1,[11,40] while other studies on the same system reported, after deconvolution, a strong peak at 199 nm and two weaker bands at 226 and 248 nm respectively.[10] However, a general agreement exists in interpreting these bands as ligand to metal charge transfer (LMCT) transitions from occupied oxygen states to empty Ti d orbitals in tetrahedral TiO_4 units.

Combination of periodic DFT calculations with the TDDFT/cluster approach provides a reliable theoretical description of electronic properties of zeolitic Ti.[35] Unless otherwise stated, the results here presented refer to TD-DFT excitations calculated for clusters extracted from optimized PBE/VDB/30 models.

The electronic excitation spectra calculated for the 12 Ti-centered C_{tetra} clusters, reported in Figures 5-6, show absorptions in the 200-230 nm region typical of experimental spectra of Ti-zeolites. In order to exclude that calculated excitations derive from artifacts of the adopted approximations, the electronic spectrum of a T1 cluster extracted from silicalite was calculated as well. By comparing the Ti- and Si- centered systems (Figure 5) it clearly emerges that the 200-230 nm band is due to tetrahedral TiO_4, in line with the current interpretation, and with previous theoretical studies.[35,36] Moreover, calculations for Ti in the T6 site performed on both C_{tetra} and C_{5-ring} clusters provided analogous electronic structure descriptions and very close wavenumbers for the lowest energy transition ($\Delta\lambda_{max}$ = 1.1 nm). Therefore, the results presented below are not significantly affected by cluster size effects.

Calculated electronic excitation spectra show different profiles but are all characterized by multiple peaks. The presence of multiple bands derives, in general, from the splitting of the empty Ti 3d and of the occupied O 2p states as a consequence of the quasi-tetrahedral T-site environment, as highlighted by previous work on different Ti-zeolites.[36] By a thorough analysis of the electronic structure in terms of the molecular orbitals involved in the excitations, a detailed description of the electronic transitions that characterize Ti in the 12 different T sites can be obtained.

In the C_{tetra} (Ti-[O-($Si(OH)_3$]$_4$) clusters, the lower energy empty molecular orbitals (MO) are mostly localized on Ti and may be described in terms of crystal field theory (CFT) in the case of tetrahedral coordination. More specifically, the two lowest empty MOs, the LUMO and LUMO+1, may be correlated with the Ti d_{z^2} and Ti $d_{x^2-y^2}$ states, while the MOs from LUMO+2 to LUMO+7 are due to combinations of Ti d_{xy}, d_{xz}, d_{yz} with framework oxygens lone pairs (Figure 7). By borrowing the familiar CFT notation, we shall refer to these two groups of states as $e_g^{(E)}$ and $t_{2g}^{(E)}$ respectively, where (E) stays for "empty". However, at difference with the case of an ideal tetrahedron, here degeneracy of the $e_g^{(E)}$ and of the $t_{2g}^{(E)}$ states is removed because TS-1

actually provides distorted tetrahedral environments to the metal center. In addition, such distortions are different for each T site, and depend not only on the local TiO_4 geometry, but are also related to Ti-Si separations, Ti-O-Si angles and, in general, to the arrangement of the SiO_4 units around Ti. This leads to slightly different orbital splitting patterns among the 12 model systems; in particular, $e_g^{(E)}$ and $t_{2g}^{(E)}$ states are separated by energy differences ranging from 0.58 eV (T10) to 0.95 eV (T8), while the LUMO-LUMO+1 separation ($e_g^{(E)}$ splitting) varies between 0.045 eV (T4) and 0.174 eV (T6).

As a first approximation, a CFT-like description could be adopted also for the 32 higher energy occupied states of the C_{tetra} models, where the dominant contribution comes from the O 2p lone pairs (two for each of the 16 O atoms). In tetrahedral symmetry, they are split in three groups, that could be labelled $t_{2g}^{(O)}$, $t_{2g}^{(O-1)}$ and $e_g^{(O)}$ in decreasing energy order (with O indicating "occupied"). These MOs contain however non negligible contributions of the Ti d orbitals. Thus, besides the details of T site geometry and symmetry, their energy ladder also depends on the extent of contamination with metal states. Actually, the details of the electronic structure in the frontier MOs region change among the 12 T site models and such variations are not straightforwardly related to simple structural parameters such as Ti-O bond distances. These observations explain why the calculated spectra differ in the number, position, and intensity of the peaks and, at the same time, suggest that determining Ti-siting simply from analysis of UV-Vis band profiles could be a very difficult task, even in the case of a non-defective TS-1. Indeed, optical spectra of systems characterized by different Ti locations share a number of common features, as detailed below.

A graphical representation of relevant orbitals is shown in Figure 7 for the case of Ti in T6. The occupied MOs involved in electronic transitions are the $t_{2g}^{(O)}$ ones. In the C_{tetra} clusters, they correspond to the 12 states from HOMO to HOMO-11, and may be grouped into two subsets. While the higher energy $t_{2g}^{(O)}$ states are basically non-

bonding O 2p combinations (nb-$t_{2g}^{(O)}$), the ones at lower energy are characterized by mixing with Ti d states and present therefore a certain degree of Ti-O bonding character (b-$t_{2g}^{(O)}$). Moreover, the frontier occupied MOs are not strictly localized on the Ti-bound oxygens, but should formally be regarded as extended over all the oxygens in the model system. Such an electronic structure description holds for larger C_{5-ring} models as well, as clearly shown in Figure 8. In particular, while the HOMO is mainly localized on the Ti-bound oxygens, other nb-$t_{2g}^{(O)}$ are delocalized over the whole 5-ring system. Therefore, by extrapolating to the solid, LMCT electronic transitions in low Ti-content TS-1 essentially go from the $t_{2g}^{(O)}$ band to the localized Ti d states.

The edge (lowest energy absorption) of the calculated spectra, ranging from 223.2 (T1) and 230.7 (T6) nm, is mainly due to the HOMO→LUMO transition, with however significant contributions from the HOMO-1→LUMO and HOMO-2→LUMO excitations. The higher wavelength peak (210-225 nm) is due to nb-$t_{2g}^{(O)} \rightarrow e_g^{(E)}$ transitions and has a pure LMCT character, while bands between 195 and 210 nm derive from b-$t_{2g}^{(O)} \rightarrow e_g^{(E)}$ transitions and might be considered LMCT contaminated by O 2p - Ti d mixing. Interestingly, the $t_{2g}^{(E)}$ states do not contribute to the bands above 200 nm because of their quite large energy separation from the $e_g^{(E)}$ ones. Indeed, absorptions below 190 nm are mainly related to lower intensity $t_{2g}^{(O)} \rightarrow t_{2g}^{(E)}$ transitions; however, in the real material, such bands should be at least partially obscured by the silica matrix absorptions.

Let us now consider the excitation spectra for the higher Ti-content TS-1 systems (Figures 9-11). It should be stressed at the outset that, also in this case, DFT/pbc and TDDFT/cluster approaches provide very close representations of electronic excitation properties, leading to similar band profiles and peak position differences in the 10 nm range (Figures 10-11).

Electronic spectra were calculated for models characterized by different arrangements of the two Ti atoms in the TS-1 cell. In particular, T site locations and Ti^1-Ti^2

separations were selected with the aim of discriminating, in the calculated spectra, the effect of the Ti content increase (Figure 9) from that of the Ti-Ti interaction (Figures 10-11).

The effect of Ti content on TS-1 electronic spectra is cleary pictured in Figure 9. Here, a $[Ti_2Si_{94}O_{192}]$ model with two Ti atoms located in two T3 sites separated by 14 Å has been considered and electronic excitations calculated with the DFT/pbc approach. Remarkably, the optical conductivity of this system amounts to twice the one calculated for $[TiSi_{95}O_{192}]$ with Ti in T3. On these basis, it could be predicted that UV-Vis spectra of TS-1 systems with well separated (non-interacting) Ti centers will be characterized by an intensity proportional to the Ti content, i.e. following the Beer-Lambert law. Closer Ti centers should lead to deviations from the Beer-Lambert behaviour. Such a prediction is confirmed by comparing electronic spectra of systems containing two close Ti atoms with those of the corresponding low-Ti content models. In the case of a representative Ti-O-Si-O-Ti structure, where Ti^1 is in T3, Ti^2 in T6 and the Ti^1-Ti^2 separation amounts to 5.605 Å, a Beer-Lambert like behaviour is still observed: intensities are approximately additive and only a small red-shift of the edge is detected (see Figure 10). Indeed, analysis of the TD-DFT excitations and of the MOs involved in the transitions indicates that the presence of two non-adjacent Ti centers perturbs but does not alter substantially the electronic structure of the TS-1 system with respect to the case of "isolated" (or well-separated) Ti centers. Therefore, the optical spectrum of a system with two TiO_4 units interconnected by a Si in close T sites could approximately be described as the sum of two spectra, each related to isolated TiO_4 in one of the sites (namely, T3 and T6). In the present case, the absorption edge corresponds to the lowest energy transition in the T6 system, while the excitation responsible of the spectral edge of the T3 system could be identified at 224.6 nm. Indeed, the orbitals involved in the UV-Vis transitions resemble the frontier orbitals of the C_{tetra} clusters with Ti in T3 and T6. For instance, the HOMO is mainly

localized on the 2p oxygens around Ti in T6, while the HOMO-1 is spread over all oxygens of the 5-ring. All of the lowest unoccupied MOs have Ti-3d character: In particular, the LUMO and LUMO+1 are mainly related to Ti d-states in T6 with a minor contribution of Ti-d in T3, while LUMO+2 is predominantly localized on T3 and slightly contaminated by Ti-d in T6. Therefore, a small degree of mixing between Ti d states is present, thus allowing partial delocalization of the lowest unoccupied MOs on nearest-neighboring Ti centers.

On the other hand, direct interaction between Ti centers like in the Ti-O-Ti bridge (Ti^1-Ti^2=3.495 Å, with Ti^1 in T3 and Ti^2 in T4) leads to a large red shift of the UV-Vis edge (to 248 nm), as well as to significant modifications in the absorption profiles (Figure 11). Such a pronounced change arises from drastic alterations in the TS-1 electronic structure. In particular, the lowest unoccupied states could no longer be described as Ti d states in a tetrahedral CFT, because the TiO_4 units forming the Ti-O-Ti moiety do share an oxygen atom and are, therefore, bonded to each other. This allows d-orbital mixing between Ti centers, with relevant consequences on both electronic excitation and bonding properties. Concerning the latter, electronic structure analysis highlighted that several low-energy MOs (not involved in optical transitions) delocalized on the Ti-O-Ti moiety contain a major contribution of Ti d states and are characterized by a pronounced bonding character in the Ti-O-Ti region (Figure 12). Such a large Ti-d participation in bonding is responsible of a particularly strong Ti-O-Ti interaction and explains why the Ti-O bond distances in the bridge are the shortest ones (see Table 3). However, d-d mixing not only stabilizes the bonding states, but its effect is even greater on the lowest unoccupied MOs, the LUMO and LUMO+1, which correspond to the arrival states of the lowest-energy electronic transitions: As a result, the edge of the excitation spectrum is redshifted.

Actually, from detailed assignment of the spectral bands it emerges that all absorptions beyond 205 nm involve excitations to the LUMO and LUMO+1 orbitals. The

absorption edge is due to the HOMO→LUMO transition, with the HOMO showing a pure non-bonding O 2p character like in the case of low Ti-content systems. However, the maximum peak (at 225 nm) is due to excitations starting from b-$t_{2g}^{(O)}$-like states where the extent of Ti-d contamination is higher than in the isolated Ti centres cases. Also at smaller wavelengths, the bands could be generally ascribed to excitations from delocalized O 2p states with smaller Ti-d character, to low energy empty states deriving from the combination of the empty d-orbitals. Interestingly, such excited states (Figure 12b,c) are spread over the Ti-O-Ti moiety and evenly localized on both Ti centres. Therefore, d-d mixing also causes excited electrons to be more delocalized with respect to the case of an isolated Ti centre.

4 Summary and conclusions

Non-defective TS-1 models have been investigated by means of periodic DFT calculations, with the aim of contributing to the issue of Ti preferential positioning. The molecular complexity underlying the TS-1 synthesis process makes it difficult to single out the factor that actually determines Ti preferential location in such a relevant material.[19] Nevertheless, from the results here presented, a non random Ti siting in TS-1 emerged on the basis of thermodynamics (energetics) considerations only.

For a Ti content corresponding to 1.35% in weight of TiO_2 (one Ti in 96 T sites) the structures with titanium siting in T3 or T4 are the most probable.

The siting problem becomes more involved for higher Ti content, here analyzed in a limited set of possible structures, corresponding to a Ti content of 2.70% in weight of TiO_2 (i.e. 2 Ti over 96 T sites). In this case, both the kind of Ti sites and their Ti-Ti separation play a relevant role for the relative stability.

Quite interestingly, the presence of a Ti-O-Ti bridge (Ti-Ti distance of 3.5 Å), where both Ti are in a tetrahedral TiO_4 geometry, is not particularly destabilized with respect to different double Ti substitutions. Actually one of such structures is only 2.7

kcal/mol higher in energy with respect to the most stable one in the sampled configurations.

Starting from the optimized periodic structures, electronic excitation spectra were obtained by adopting a cluster approach and a TD-DFT calculation scheme. All of the different Ti sites present absorption profiles in the 200-230 nm UV region in line with DRUV-Vis experiments on low Ti content dry TS-1 samples. The excitations present a multiband profile which is characteristic of each different T site. The actual profiles are strictly interlaced with distortion from the perfect tetrahedral symmetry which is different for different crystallographic sites. The absorption bands involve transitions from oxygen lone pairs to empty d-states localized on Ti (i.e. LMCT: ligand to metal charge transfer transitions), in line with the current opinion.

Our results however suggest a description more complex than the standard picture, based on $O^{2-}+Ti^{4+} \rightarrow O^{-}+Ti^{3+}$ transitions involving only Ti-bound oxygen atoms. Actually, we propose that UV-Vis transitions in titanium zeolites would occur from framework oxygens bands to localized Ti empty states. The participation of extended electronic structures to the UV transitions in Ti zeolites may be a key point in explaining the photoconducting properties recently highlighted in Ti zeolites (TS-1 included).[3] Besides electronic excitations, analysis of the vibrational properties has been performed. From the investigations on isolated Ti sites a picture in line with previous analysis emerges: the 960 cm^{-1} band in the IR transparent silica window can be associated to tetrahedral Ti, along with a raman active feature detected at 1125 cm^{-1}. Some interesting features however emerged from the vibrational spectra of Ti-O-Si-O-Ti and Ti-O-Ti bridges. Associated to the first structure, we have found an IR active band just in the center of the silica window, at 908 cm^{-1}, that could be easily detectable in the experimental IR spectra. The absence of such a band in the available IR spectra of TS-1 indicates that the presence of such a structure can be excluded in real TS-1. More problematic could be the clear-cut exclusion of a Ti-O-Ti bridge: in-

deed this structure gives IR signatures (853 and 1003 cm^{-1}) which are just at the edge of the silica window. Also an intense raman active mode calculated at 1115 cm^{-1} can be compatible with the tetrahedral Ti "raman signature" at 1125 cm^{-1}. Moreover its calculated absorption edge at 248 nm is compatible with available TS-1 data. Probably such a (tetrahedral Ti) Ti-O-Ti structure could be considered a nucleation center for the (octahedral Ti) TiO_2 phase separation. Indeed, for the TiO_2 phase growth, which is known to occur at Ti contents higher than 2.5%, Ti-O-Ti bridges should be formed. Our results, which demonstrate the stability of this moiety in models of comparable Ti content, its compatibility with available spectroscopic data and its peculiar electronic properties, suggest therefore further experimental work aimed at the identification and characterization of Ti-O-Ti bridges in the TS-1 framework.

	ΔE	Ti-O	Ti-O	Ti-O	Ti-O	<Ti-O>
T1	5.59	1.7855	1.7928	1.7955	1.7965	1.7926
T2	3.87	1.7912	1.7914	1.7971	1.7984	1.7945
T3	0.0	1.7827	1.7905	1.7931	1.8040	1.7925
T4	0.28	1.7895	1.7965	1.7971	1.7989	1.7955
T5	2.84	1.7935	1.8006	1.8013	1.8030	1.7996
T6	4.92	1.7919	1.7952	1.7959	1.8039	1.7967
T7	4.06	1.7881	1.7936	1.7962	1.8085	1.7966
T8	2.29	1.7778	1.7934	1.7959	1.8105	1.7944
T9	2.23	1.7803	1.7978	1.7987	1.8042	1.7953
T10	4.20	1.7923	1.7951	1.7969	1.8039	1.7971
T11	1.41	1.7929	1.7943	1.8041	1.8096	1.8002
T12	1.48	1.7867	1.7917	1.8023	1.8048	1.7964

Table 1: Calculated ΔE (in kcal/mol), optimized Ti-O bond distances and average <Ti-O> distances *vs.* T site. Distances in Å.

							<OTiO>
T1	108.7	113.3	111.0	107.5	108.6	107.6	109.4
T2	108.2	107.8	110.3	107.5	112.5	110.4	109.4
T3	109.9	108.0	110.5	107.3	109.5	111.6	109.5
T4	110.3	105.6	112.0	108.3	109.7	110.9	109.5
T5	110.5	106.6	108.8	109.9	108.6	112.3	109.5
T6	109.0	109.8	109.4	110.8	106.9	110.9	109.5
T7	108.1	108.5	109.9	108.2	112.2	109.7	109.5
T8	109.0	108.6	106.9	111.5	108.7	112.0	109.4
T9	110.0	109.4	110.1	106.1	110.5	110.6	109.5
T10	109.4	110.3	109.6	108.3	109.7	109.5	109.5
T11	107.4	108.8	110.9	108.6	110.6	110.4	109.5
T12	108.7	109.3	112.0	110.1	109.4	107.2	109.5

Table 2: Optimized O-Ti-O bond angles and average O-Ti-O bond angle (<OTiO>) *vs.* T site. Angles in degrees.

	Ti-Ti	Ti-O*	Ti-O	Ti-O	Ti-O	<Ti-O>
T3	3.4952	1.7761	1.7949	1.7978	1.8016	1.7918
T4	3.4952	1.7870	1.7934	1.7940	1.7976	1.7930

Table 3: Optimized Ti-Ti separation and Ti-O bond distances for a [$Ti_2Si_{94}O_{192}$] structure characterized by Ti in T3 and T4 with a Ti-O-Ti bridge. The Ti-O* entry refers to the Ti-O-Ti bonds. Distances in Å.

							<OTiO>
T3	106.1	108.1	108.3	109.6	111.8	112.6	109.4
T4	106.2	106.9	108.6	109.1	111.8	114.1	109.5

Table 4: Optimized O-Ti-O bond angles and average O-Ti-O bond angle (<OTiO>) for a [$Ti_2Si_{94}O_{192}$] structure characterized by Ti in T3 and T4 with a Ti-O-Ti bridge. Angles in degrees.

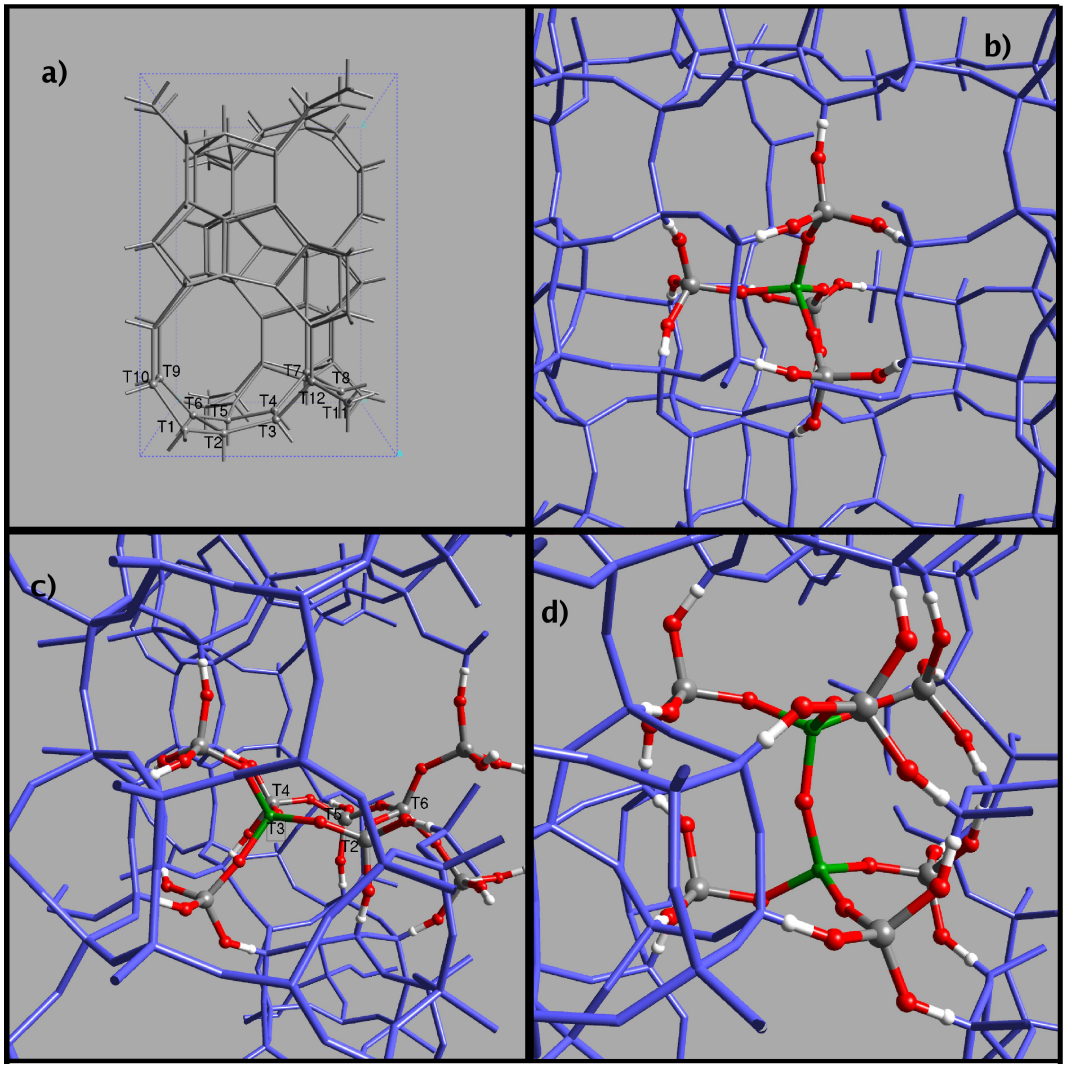

Figure 1: a) Graphical representation of the MFI unit cell. Only T atoms are represented. Also reported are the labels of the twelve independent T sites. b) Ball-and-stick Ti[O-(Si(OH)$_3$]$_4$ cluster (C_{tetra}) superimposed on the TS-1 crystal (blue sticks). Color codes: Si, gray spheres; O, red spheres; H, white spheres; Ti, green sphere. c) Ball-and-stick representation of a C_{5-ring} cluster superimposed on the TS-1 crystal (blue sticks). Color codes: Si, gray spheres; O, red spheres; H, white spheres; Ti, green sphere. d) Ball-and-stick representation of a Ti-O-Ti bridge structure (C_{2tetra} cluster) superimposed on the TS-1 crystal (blue sticks). Color codes: Si, gray spheres; O, red spheres; H, white spheres; Ti, green spheres.

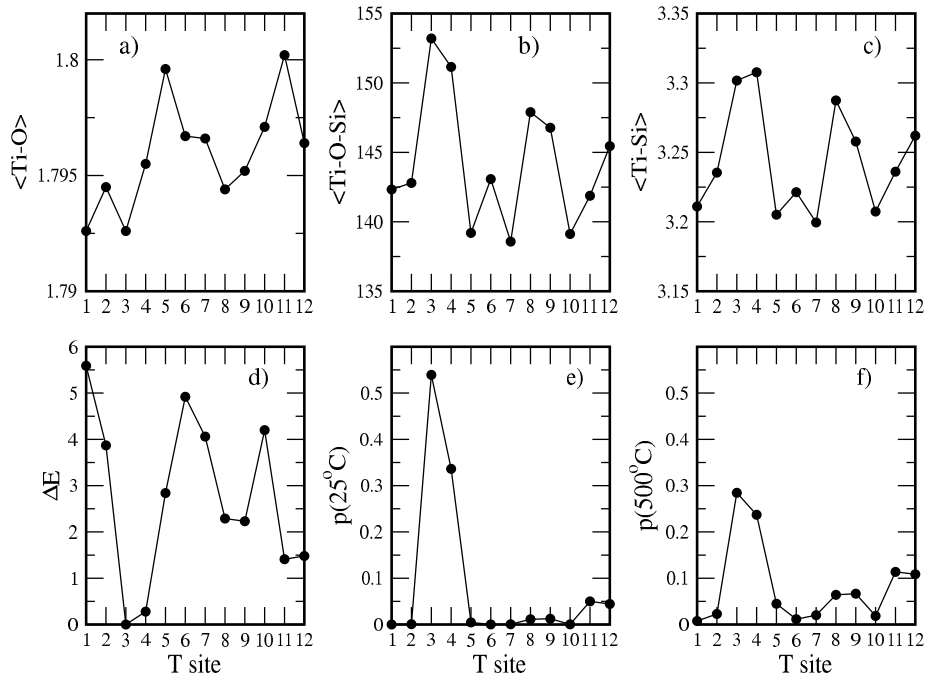

Figure 2: Selected properties of $[TiSi_{95}O_{192}]$ characterized by different siting of Ti. a): average Ti-O bond distances (in Å) for different Ti siting. b): average Ti-O-Si angles (in degrees) for different Ti siting. c): average Ti-Si separation (in Å) for different Ti siting. d): PBE/VDB/30 ΔE (in kcal/mol) calculated with respect to Ti in T3. e): normalized probability of occurrence of Ti in the 12 T sites at 25 °C. f): normalized probability of occurrence of Ti in the 12 T sites at 500 °C.

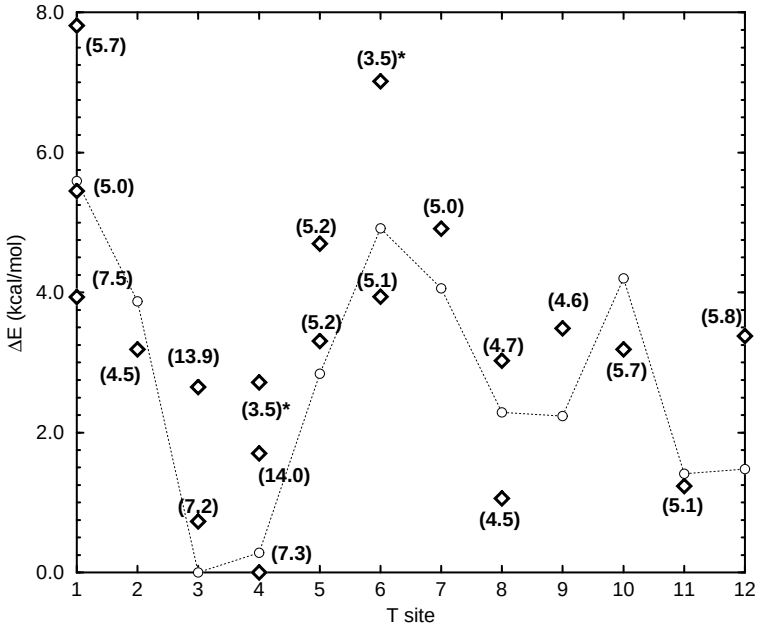

Figure 3: Energy differences ΔE in kcal/mol of selected $[Ti_2Si_{94}O_{192}]$ configurations. In all configurations, Ti^1 is positioned in T3. They differ by the siting of Ti^2. The diamonds represent the energy relative to the most stable configuration among the sampled ones (Ti^1 in T3 and Ti^2 in T4), with the corresponding Ti^1-Ti^2 distance (in Å) reported in parenthesis. Configurations labeled with a star are characterized by a Ti-O-Ti bridge. Circles connected by a dashed line represent the energy scale for a single Ti substitution ($[TiSi_{95}O_{192}]$).

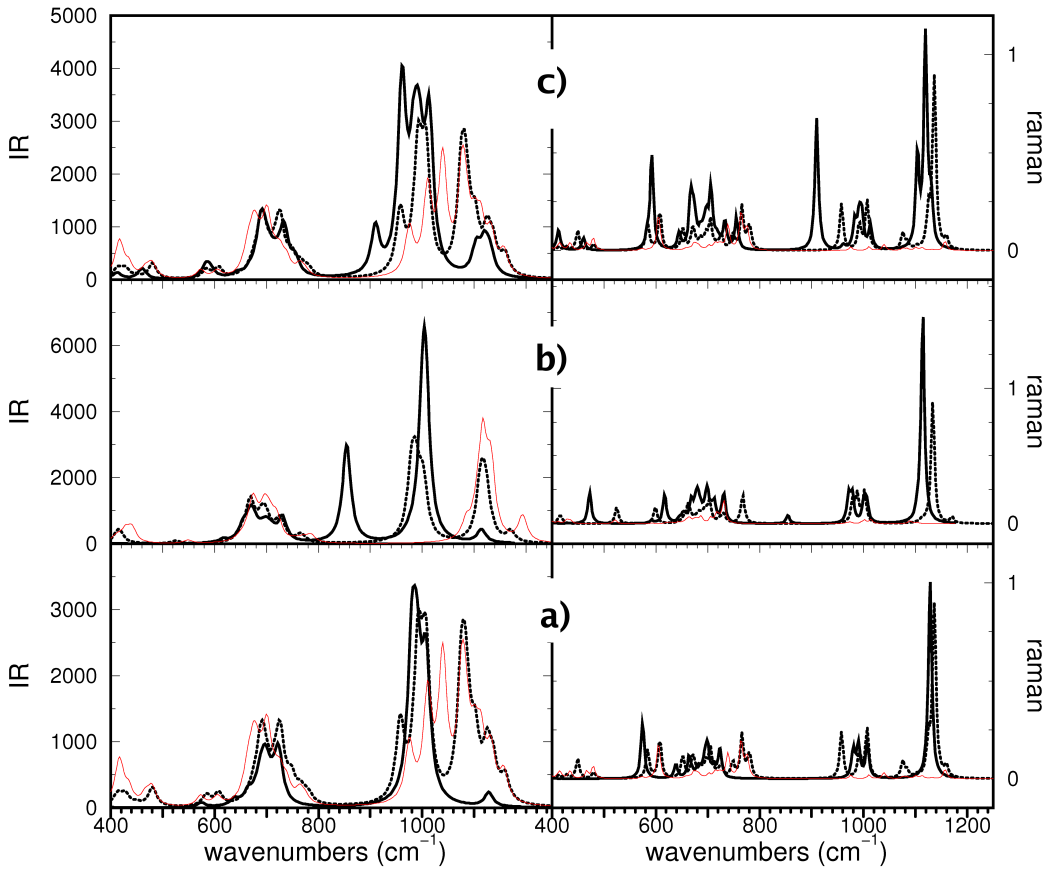

Figure 4:
Calculated IR (left panels) and raman (right panels) intensities. a) thick-line: C_{tetra} with Ti in T3; dashed-line: C_{5-ring} with Ti in T3; red-line: all silica C_{5-ring}. b) thick-line: C_{2tetra} with a Ti-O-Ti bridge, Ti in T3 and T4; dashed-line: C_{2tetra} with one Ti in T3; red-line: all silica C_{2tetra}. c) thick-line: C_{5-ring} with a Ti-O-Si-O-Ti bridge, Ti in T3 and T6; dashed-line: C_{5-ring} with one Ti in T6; red-line: all silica C_{5-ring}.

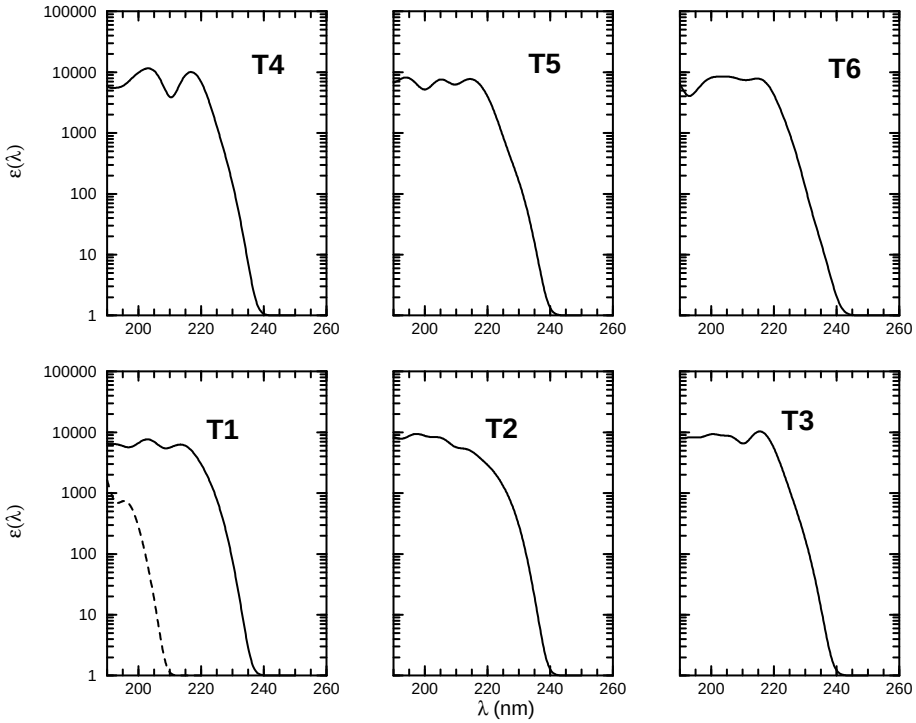

Figure 5: Calculated TD-DFT excitation spectra of cluster models cut from $[Ti_1Si_{95}O_{192}]$ DFT optimized structures. Calculated spectra are relative to C_{tetra} with Ti in the T1, T2, T3, T4, T5 and T6 sites. The excitation spectrum for a C_{tetra} all silica cluster (site T1) is reported for comparison (dashed line).

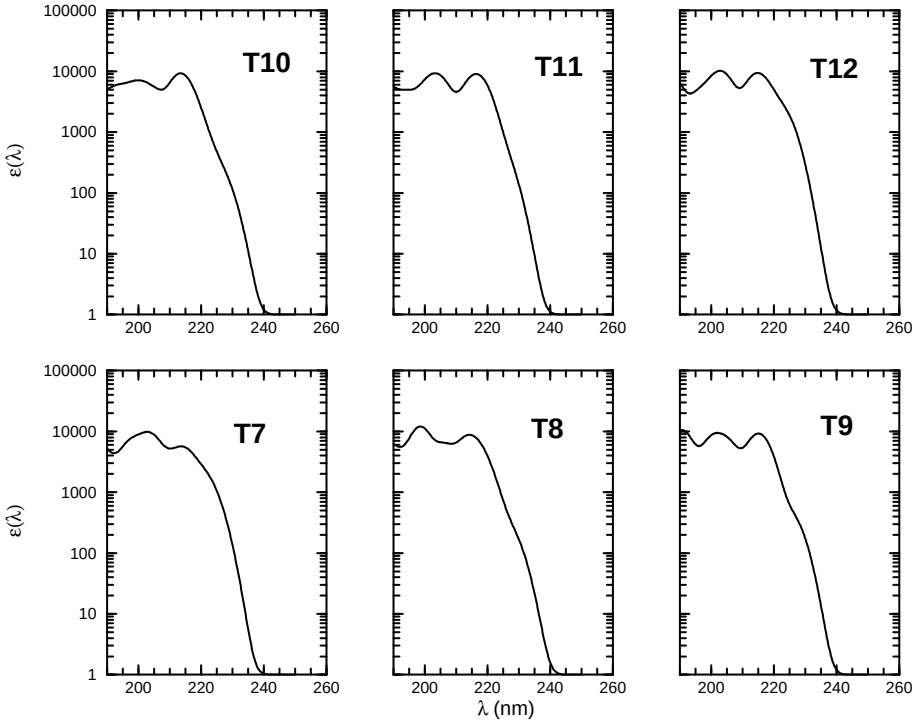

Figure 6: Calculated TD-DFT excitation spectra of cluster models cut from $[Ti_1Si_{95}O_{192}]$ DFT optimized structures. Calculated spectra are relative to C_{tetra} with Ti in the T7, T8, T9, T10, T11 and T12 sites.

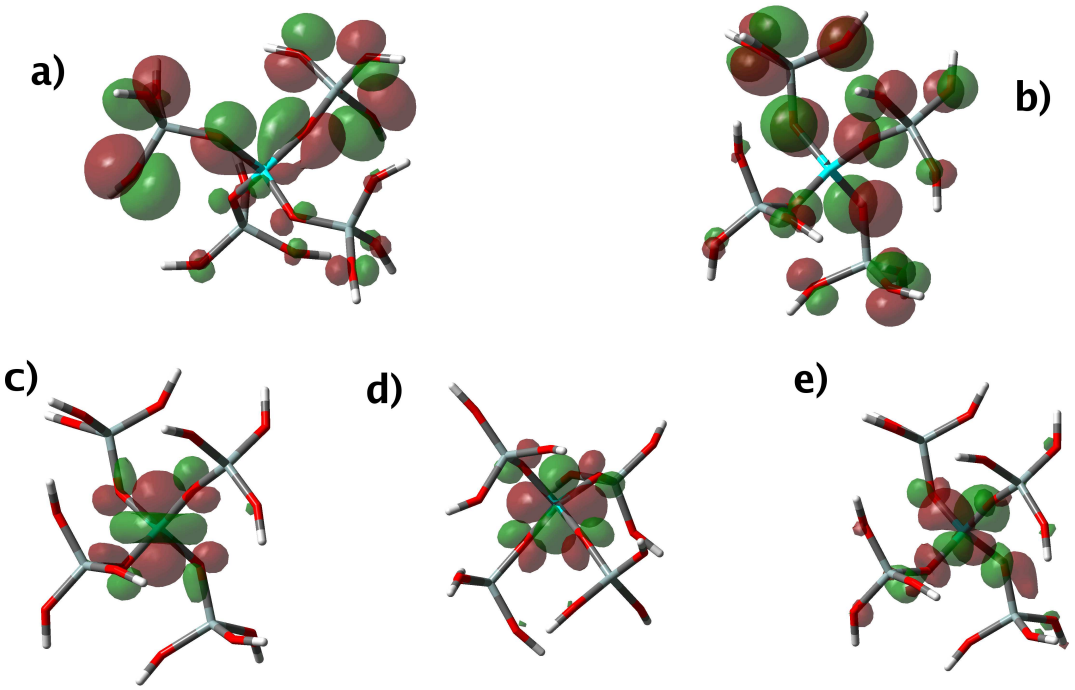

Figure 7: Representative examples of frontier molecular orbitals involved in electronic transitions in one C_{tetra} (Ti-(O-Si(OH)$_3$)$_4$) cluster, Ti in T6. a) b-$t_{2g}^{(O)}$ occupied orbital; b) nb-$t_{2g}^{(O)}$ occupied orbital; c) $e_g^{(E)}$ unoccupied orbital; d) $e_g^{(E)}$ unoccupied orbital; e) $t_{2g}^{(E)}$ unoccupied orbital. Green and red contours represent positive and negative orbital lobes. Atoms color codes: Ti, cyan; Si, gray; O, red; H, white.

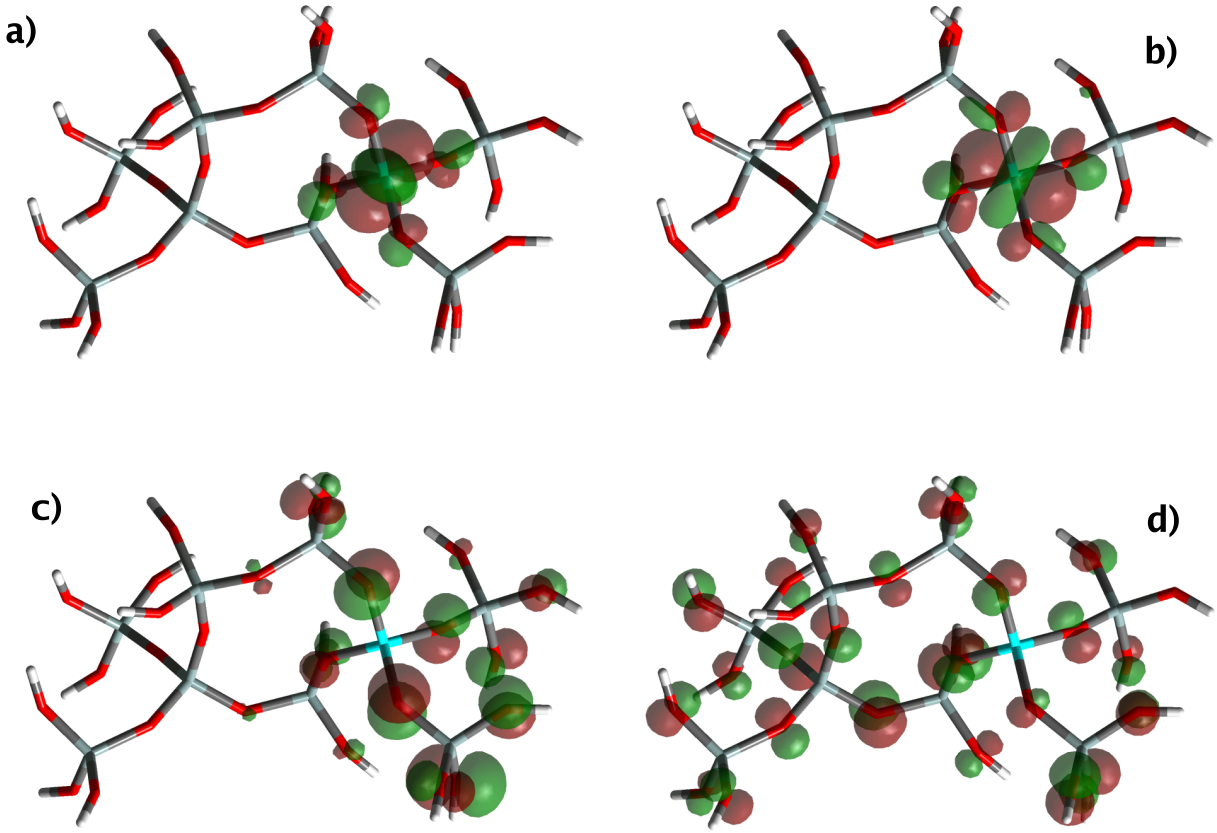

Figure 8: Representative examples of frontier molecular orbitals involved in electronic transitions for a C_{5-ring} structure with one Ti (in T6). a) $e_g^{(E)}$ unoccupied orbital; b) $e_g^{(E)}$ unoccupied orbital. c) nb-$t_{2g}^{(O)}$ occupied orbital (HOMO); d) nb-$t_{2g}^{(O)}$ occupied orbital. Color codes as in Figure 7.

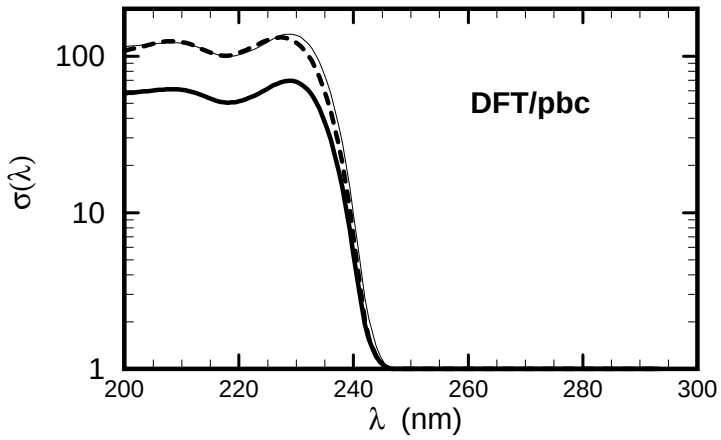

Figure 9: DFT optical conductivity σ calculated for crystal structures (with pbc). Thick line: $[Ti_1Si_{95}O_{192}]$ structure with one Ti in T3; thick-dashed line: $[Ti_2Si_{94}O_{192}]$ structure with Ti in two well separated T3 sites (Ti-Ti distance = 14.0 Å) Thin line: twice the optical conductivity σ calculated for the $[Ti_1Si_{95}O_{192}]$ structure with one Ti in T3.

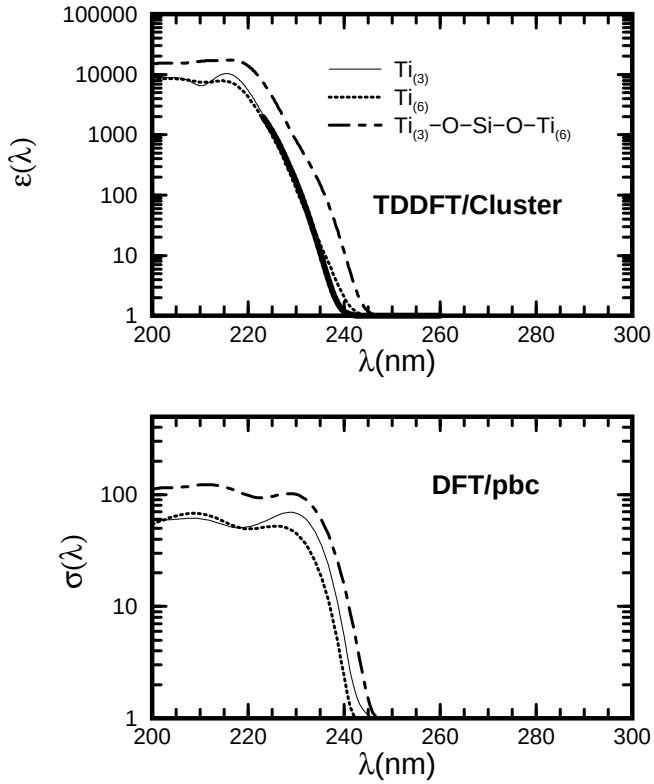

Figure 10: Top: TD-DFT absorbance spectra calculated for cluster models. Thin-line: C_{tetra} cluster with Ti in T3; thick-dotted-line: C_{tetra} cluster with Ti in T6; thick-dot-dashed line C_{5-ring} with a Ti-O-Si-O-Ti bridge, Ti in T3 and T6 cut from $[Ti_2Si_{94}O_{192}]$ Bottom: DFT optical conductivity σ calculated for crystal structures (with pbc). Thin black line: $[TiSi_{95}O_{192}]$ with Ti in T3; thick-dashed line: $[TiSi_{95}O_{192}]$ with Ti in T6; thick-dot-dashed line: $[Ti_2Si_{94}O_{192}]$ system with Ti^1 in T3 and Ti^2 in T6.

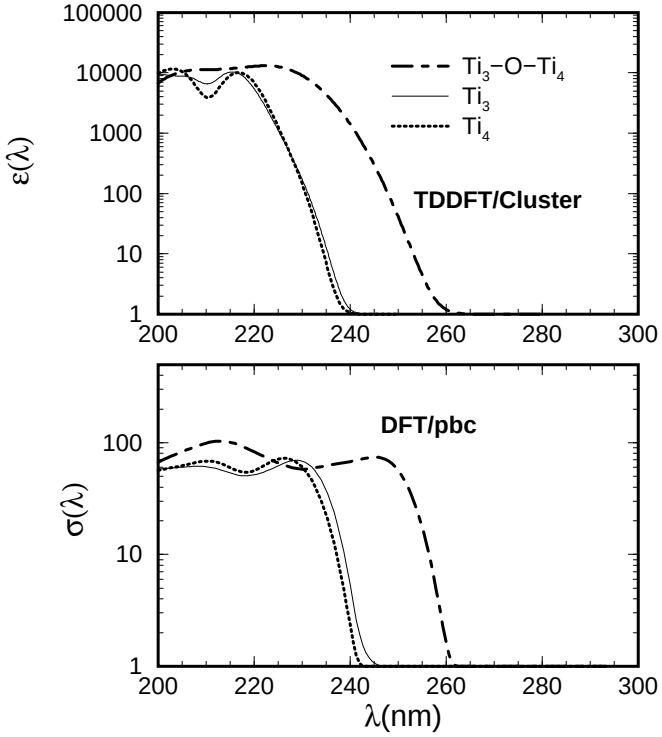

Figure 11: Top: TD-DFT absorbance spectra calculated for cluster models cut from $[Ti_1Si_{95}O_{192}]$ with Ti in T3 (thin line) and T4 (thick dotted line) and from a $[Ti_2Si_{94}O_{192}]$ with Ti both in T3 and T4 corresponding to a Ti-O-Ti structure. Bottom: DFT optical conductivity calculated for the crystal structures (with pbc). Thin black line: one Ti in T3; thick-dashed line: one Ti in T4; thick-dot-dashed line: double Ti substitution in both T3 and T4.

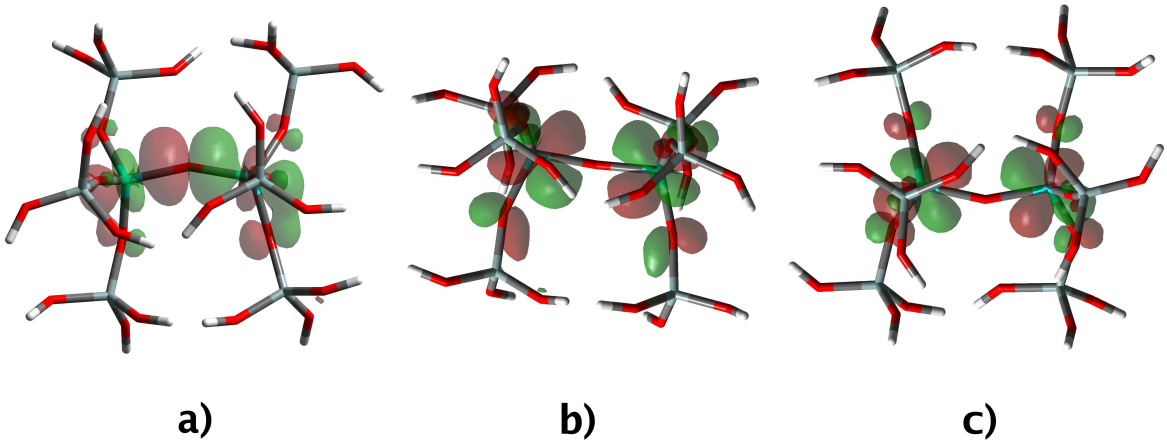

Figure 12: Relevant molecular orbitals in a cluster model containing a Ti-O-Ti bridge. a) bonding MO with dominant d_{z^2} character; b) LUMO, formed by combination of Ti-d states from both Ti centers; c) LUMO+1, formed by combination of Ti-d states from both Ti centers. Color codes as in Figure 7.

References

1. Clerici, M. G.; Bellussi, G.; Romano, U. *J. Catal.* **1991,** *129,* 159.

2. Taramasso, M.; Perego, G.; Notari, B. *US Patent 441051* **1983,** .

3. Atienzar, P.; Valencia, S.; Corma, A.; Garcia, H. *ChemPhysChem* **2007,** *8,* 1115.

4. Baerlocher, C.; Meier, W. M.; Olson, D. H. *Atlas of Zeolite Framework Types;* Elsevier: The Netherlands, 2001.

5. van Köningsveld, H.; van Bekkum, H.; Jansen, J. C. *Acta Crystallogr. B* **1987,** *43,* 127.

6. Millini, R.; Perego, G.; Berti, D.; Parker, W. O.; Carati, A.; Bellussi, G. *Micropor. Mesopor. Mater.* **2000,** *35-36,* 387.

7. Millini, R.; Previdi Massara, E.; Perego, G.; Bellussi, G. *J. Catal* **1992,** *137,* 497.

8. Scarano, D.; Zecchina, A.; Bordiga, S.; Geobaldo, F.; Spoto, G.; Petrini, G.; Leofanti, G.; Padovan, M.; Tozzola, G. *J. Chem. Soc. FARADY TRANS.* **1993,** *89,* 4123.

9. Li, C.; Xiong, G.; Xin, Q.; Liu, J.; Ying, P.; Feng, Z.; Li, J.; Yang, W.; Wang, Y.; Wang, G.; Liu, X.; Lin, M.; Wang, X.; Min, E. *Angew. Chem. Int. Ed.* **1999,** *38,* 2320.

10. Le Noc, L.; Trong On, D.; Solomykina, S.; Echchahed, B.; Beland, F.; Cartier Dit Moulin, C.; Bonneviot, L. *Stud. Surf. Sci. Catal.* **1996,** *101,* 611.

11. Lamberti, C.; Bordiga, S.; Arduino, D.; Zecchina, A.; Geobaldo, F.; Spanó, G.; Genoni, F.; Petrini, G.; Carati, A.; Villain, F.; Vlaic, G. *J. Phys. Chem. B* **1998,** *102,* 6382.

12. Lamberti, C.; Bordiga, S.; Zecchina, A.; Artioli, G.; Marra, G.; Spanó, G. *J. Am. Chem. Soc.* **2001,** *123,* 2204.

13. Hijar, C. A.; Jacubinas, R. M.; Eckert, J.; Henson, N. J.; Hay, P. J.; Ott, K. C. *J. Phys. Chem. B* **2000,** *104,* 12157.

14. Henry, P. F.; Weller, M. T.; Wilson, C. C. *J. Phys. Chem. B* **2001,** *105,* 7452.

15. Deka, R. C.; Nasluzov, V. A.; Ivanova Shor, E. A.; Shor, A. M.; Vayssilov, G. N.; Rösch, N. *J. Phys. Chem. B* **2005,** *109,* 24304.

16. Ricchiardi, G.; de Man, A. J. M.; Sauer, J. *Phys. Chem. Chem. Phys.* **2000,** *2,* 2195.

17. Sastre, G.; Corma, A. *Chem. Phys. Lett.* **1999,** *302,* 447.

18. Millini, R.; Perego, G.; Seiti, K. *Stud. Surf. Sci. Catal.* **1994,** *84,* 2123.

19. Parker, W. O.; Millini, R. *J. Am. Chem. Soc.* **2006,** *128,* 1450.

20. Boccuti, M. R.; Rao, K. M.; Zecchina, A.; Leofanti, A.; Petrini, G. *Stud. Surf. Sci. Catal.* **1988,** *48,* 133.

21. Perdew, J. P.; Burke, K.; Ernzerhof, M. *Phys. Rev. Lett.* **1996,** *77,* 3865-3868.

22. Vanderbilt, D. *Phys. Rev. B* **1990,** *41,* 7892.

23. He, Y.; Tilocca, A.; Dulub, O.; Selloni, A.; Diebold, U. *Nature Mat.* **2009,** *8,* 585.

24. Tilocca, A.; Fois, E. *J. Phys. Chem. C* **2009,** *113,* 8683.

25. Trudu, F.; Tabacchi, G.; Gamba, A.; Fois, E. *J. Phys. Chem. A* **2007,** *111,* 11626.

26. Trudu, F.; Tabacchi, G.; Gamba, A.; Fois, E. *J. Phys. Chem. C* **2008,** *112,* 15394.

27. *CPMD code;* (www.cpmd.org): Copyright MPI für Festkörperforschung, Stuttgart, and IBM Zürich Research Laboratory, 1990-2006.

28. Runge, E.; Gross, E. K. *Phys. Rev. Lett.* **1984,** *52,* 997.

29. Casida, M. E.; Jamorsky, C.; Casida, K. C.; Salahub, D. R. *J. Chem. Phys.* **1998,** *108,* 4439.

30. Becke, A. D. *J. Chem. Phys.* **1993,** *98,* 5648.

31. Frisch, M. J. *et al. Gaussian 03, Revision D.02;* Gaussian, Inc.: Wallingford CT, 2004.

32. Kleinman, L.; Bylander, D. M. *Phys.Rev.Lett* **1982,** *48,* 1425.

33. Troullier, N.; Martins, J. L. *Phys.Rev. B* **1991,** *43,* 1993.

34. Spanó, E.; Tabacchi, G.; Gamba, A.; Fois, E. *J. Phys. Chem. B* **2006,** *110,* 21651-21661.

35. Fois, E.; Gamba, A.; Tabacchi, G. *ChemPhysChem* **2005,** *6,* 1237.

36. Fois, E.; Gamba, A.; Tabacchi, G. *ChemPhysChem* **2008,** *9,* 538.

37. Scott, A. P.; Radom, L. *J. Phys. Chem.* **1996,** *100,* 16502.

38. Ricchiardi, G.; Damin, A.; Bordiga, S.; Lamberti, C.; Spano', G.; Rivetti, F.; Zecchina, A. *J. Am. Chem. Soc.* **2001,** *123,* 11409.

39. Bordiga, S.; Coluccia, S.; Lamberti, C.; Marchese, L.; Zecchina, A.; Boscherini, F.; Buffa, F.; Genoni, F.; Leofanti, G.; Petrini, G.; Vlaic, G. *J. Phys. Chem.* **1994,** *98,* 4125.

40. Fan, W.; Duan, R.-G.; Yokoi, T.; Wu, P.; Kubota, Y.; Tatsumi, T. *J. Am. Chem. Soc.* **2008,** *130,* 10150.